Archaeal cells share common size control with bacteria despite noisier growth and division

Ye-Jin Eun¹, Po-Yi Ho², Minjeong Kim¹, Salvatore LaRussa⁴, Lydia Robert^{5,6,7}, Lars D. Renner¹, Amy Schmid⁸, Ethan Garner¹, and Ariel Amir²

In nature, microorganisms exhibit different volumes spanning six orders of magnitude¹. Despite their capability to create different sizes, a clonal population in a given environment maintains a uniform size across individual cells. Recent studies in eukarvotic and bacterial organisms showed that this homogeneity in cell size can be accomplished by growing a constant size between two cell cycle events (that is, the adder model²⁻⁶). Demonstration of the adder model led to the hypothesis that this phenomenon is a consequence of convergent evolution. Given that archaeal cells share characteristics with both bacteria and eukaryotes, we investigated whether and how archaeal cells exhibit control over cell size. To this end, we developed a soft-lithography method of growing the archaeal cells to enable quantitative time-lapse imaging and single-cell analysis, which would be useful for other microorganisms. Using this method, we demonstrated that Halobacterium salinarum, a hypersaline-adapted archaeal organism, grows exponentially at the single-cell level and maintains a narrowsize distribution by adding a constant length between cell division events. Interestingly, the archaeal cells exhibited greater variability in cell division placement and exponential growth rate across individual cells in a population relative to those observed in Escherichia coli6-9. Here, we present a theoretical framework that explains how these larger fluctuations in archaeal cell cycle events contribute to cell size variability and control.

Previous work suggests that individual cells within clonal populations maintain a uniform size at a steady state with typical coefficients of variation (CV) of 10-20%10. Although the biological processes responsible for this homogeneity in cell size are not well understood, three prominent models provide a phenomenological explanation³ (see Supplementary Notes Section 1): (1) 'sizer', which proposes that cells grow to a critical size threshold prior to division; (2) 'timer', which states that cells grow for a constant amount of time between birth and division; and (3) 'adder' (or 'incremental') model, which proposes that cells add a constant volume between two cell cycle events. Recent studies have demonstrated that the adder model explains cell size control in several different bacterial organisms, including Escherichia coli^{2,4-6}, Bacillus subtilis⁶, Pseudomonas aeruginosa¹ and Desulfovibrio vulgaris¹¹. In the case of the bacteria Caulobacter crescentus, it was established that growth is exponential^{5,12}; however, whether its cell size control can be explained by the adder paradigm alone⁵, or by a mixture of adder and timer models, is currently under debate¹³. For eukaryotes, it was shown that diploid daughter cells of the budding yeast *Saccharomyces cerevisiae*² follow the adder model, whereas cells of the yeast *Schizosaccharomyces pombe* do not¹⁴. Together, these studies suggest that several evolutionarily divergent organisms have evolved the adder strategy, despite distinct underlying molecular mechanisms². However, control of cell size in archaea, the third domain of life, remains unknown.

Here, we address cell size control in archaea, which resemble bacterial cells in terms of size and shape, whereas the cell cycle events (that is, DNA replication, cell growth and division) possess features that are hybrid between eukaryotes and prokaryotes¹⁵⁻²¹. For example, several archaeal proteins involved in replication, transcription and translation are homologous to eukaryotic counterparts, whereas many archaeal genomes comprise single circular chromosomes and are organized into operons similar to bacterial genomes¹⁹. However, unlike bacterial chromosomes that harbour a single replication origin, archaeal chromosomes often have multiple origins, and their replication is initiated by Orc1-Cdc6, similar to eukaryotic cells¹⁷. Archaea display a mix of cell division and cytoskeletal proteins, depending on the phylum: the genome of representatives of the crenarchaeal phylum and the Asgard superphylum encodes proteins homologous to endosomal sorting complexes required for transport (ESCRT) and actins in eukaryotes, whereas many species of the euryarchaeal phylum possess bacterial counterparts, such as ftsZ, minD and mreB18,19,22.

Given the ancestral nature of the archaeal domain, development of a phenomenological model of the cell cycle for this domain is critical for understanding the evolution and conservation of cell size and cell cycle control²³. To this end, single-cell observations of growth and division are required; however, it has been difficult to obtain data with high temporal resolution due to the extreme conditions that are required for cell viability of many archaeal model organisms (for example, near-saturating levels of salinity)¹⁶.

We studied the hypersaline-adapted model archaeon *Halobacterium salinarum*, which maintains rod shape when grown freely in liquid media with an optimum salt concentration across different growth phases (Supplementary Table 1). The rod shape of *H. salinarum* makes it possible to use length and two-dimensional (2D) area as a proxy for volume. However, we noted that growth under even a moderately stiff agarose gel (2% w/v) causes *H. salinarum* rods to grow as flat polygons or amorphous shapes (Supplementary Fig. 1). This is unlike many bacterial and fungal

¹Department of Molecular and Cellular Biology, Center for Systems Biology, Harvard University, Cambridge, MA, USA. ²School of Engineering and Applied Sciences, Harvard University, Cambridge, MA, USA. ³Leibniz Institute of Polymer Research and the Max Bergmann Center of Biomaterials, Dresden, Germany. ⁴Masconomet Regional High School, Boxford, MA, USA. ⁵INRA, UMR 1319 Micalis, Jouy-en-Josas, France. ⁶AgroParisTech, UMR Micalis, Jouy-en-Josas, France. ⁷Laboratoire Jean Perrin, UPMC-CNRS, UMR 8237, UPMC, Paris, France. ⁸Biology Department, Center for Genomics and Computational Biology, Duke University, Durham, NC, USA. *e-mail: amy.schmid@duke.edu; egarner@g.harvard.edu; arielamir@seas.harvard.edu

LETTERS NATURE MICROBIOLOGY

model organisms with rigid cell walls, suggesting that H. salinarum cells are more sensitive to mechanical stress. Because of this sensitivity, we developed microfabricated agarose chambers to cultivate H. salinarum, allowing us to visualize and track hundreds of cells with high temporal and spatial resolution for up to four generations and up to eight total cell divisions per agarose chamber (Fig. 1a,b and Supplementary Video 1). Cells in agarose chambers maintained their rod shape and grew at a rate similar to aerated cells in batch culture (a mean doubling time of 6h (±1, s.d.) at 37°C; 3 independent trials with 5 replicates each). We also found that there were no systematic changes in the cell cycle that depend on the generations when grown in the agarose chambers (Supplementary Fig. 2a,b). Furthermore, we verified that there was no variation between the independent trials in the agarose chambers (Supplementary Table 2 and Supplementary Fig. 3). In Supplementary Notes Section 6, we provide details of other cultivation methods that were attempted unsuccessfully.

We found the diameter CV to be small (12%; n=92), which allowed us to use the length of rod-shaped cells as a proxy for cell volume. While we report our main findings here using measurements of cell length, duplicate analysis using the 2D area data provides identical conclusions (Supplementary Fig. 4).

As understanding the growth pattern is critical for investigating size control, we first asked whether cells grow at a constant rate (linear) or at a rate that is proportional to their size (exponential). One method to determine exponential growth is to measure and plot the size of individual cells over time, and then fit an exponential function to hundreds of individual plots of single-cell growth. Instead of this approach, which requires high measurement precision, we treated single-cell growth data as individual points in a scatter plot (Fig. 1c and Supplementary Fig. 4a), and used the entire data to fit only once to determine exponential growth (see below for details)². Thus, this approach uses the power of statistics (that is, averaging) to negate the need for having a very high precision for cell size measurements.

For an exponentially growing single cell, the time taken between divisions (that is, the interdivision time, t_d) and birth size (l_{birth}) are related to the division size (l_{division}):

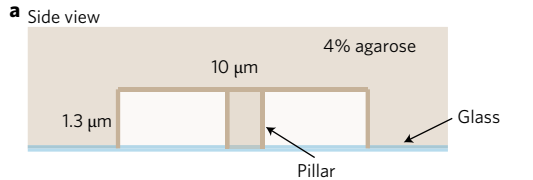
$$l_{\text{division}} = l_{\text{birth}} e^{\lambda t_{\text{d}}} \tag{1}$$

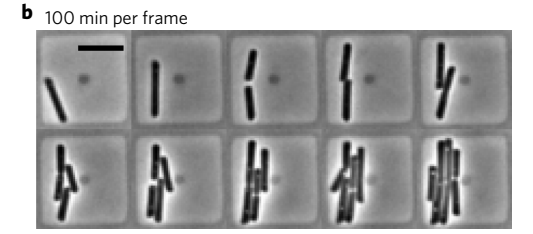
where λ is the exponential growth rate constant. Rearranging equation (1), we obtain:

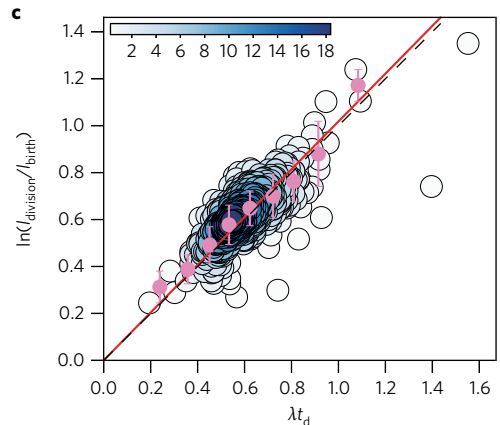
$$\ln\left(\frac{l_{\text{division}}}{l_{\text{birth}}}\right) = \lambda t_{\text{d}} \tag{2}$$

yielding a linear relationship with a slope of 1 and an intercept of 0. Fitting the data for cell length with equation (2) representing exponential growth (Fig. 1c), we detected a significant relationship with a slope of 1.018 ± 0.007 (s.e.; P<0.001, $R^2=0.978$). Similarly, fitting the 2D area data (Supplementary Fig. 4a) gave a slope of 0.992 ± 0.008 (s.e.; P<0.0001). Furthermore, we found that the experimental setup using agarose chambers does not influence the exponential growth mode of H.salinarum (Supplementary Fig. 2c). Conversely, we found that a linear growth model does not fit the data well (Supplementary Fig. 5 and Supplementary Notes Section 7). Overall, these results demonstrated that single H.salinarum cells grow exponentially (Fig. 1c and Supplementary Fig. 4a), similar to certain bacterial and fungal cells⁸.

We then sought to determine whether and how cell size is controlled in *H. salinarum*. Live-cell imaging indicated that cell length distributions at birth and division have a CV of 16% and 13%, respectively, suggesting that *H. salinarum* maintains cell size homogeneity during the exponential phase while roughly doubling in size







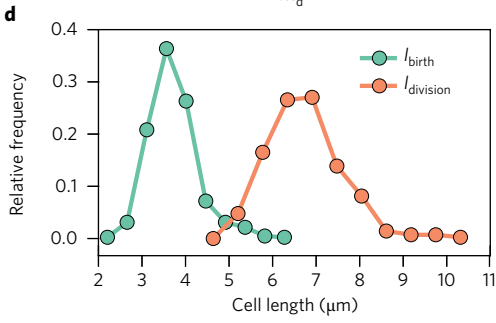


Fig. 1 | H. salinarum cells grow exponentially, and their lengths at birth and division are narrowly distributed. a, Schematic of the architecture and dimensions of the agarose microchambers. The microchambers contained a relatively much softer low-melting agarose (0.3% w/v) to restrict free swimming of H. salinarum cells. b, Montage of a typical time-lapse (see Supplementary Video 1) taken using microchambers (video taken every 5 min; not all frames are shown). This montage represents three experiments. Scale bar, 5 μm. c, Single H. salinarum cells grow exponentially. We pooled data from three independent trials. The ratio of I_{birth} and I_{division} after natural log transformation was plotted against t_d normalized by λ (0.117 h⁻¹), which was independently measured by bulk culture growth measurements rather than being a fitted parameter. Unless otherwise noted, experimental data acquired using microchambers are visualized as combinations of scatter plots and probability density heatmaps. The colour bar inset shows the densities for the heatmap. Data points after binning along the x axis are overlaid: the mean and standard deviation of each bin are plotted as pink circles and error bars, respectively. Linear regression of raw data (red solid line) yields a slope of 1.018 ± 0.007 (s.e.; n = 418, P < 0.001 for the null hypothesis that the slope is zero). A black dashed line with a slope of 1 is overlaid for comparison. d, Histogram of H. salinarum cell lengths show narrow distributions (pooled from three experiments) around the mean of $3.5 \,\mu\text{m}$ (CV = 16%; n = 418) and $6.5 \,\mu\text{m}$ (CV = 13%; n = 418) for birth and division, respectively.

NATURE MICROBIOLOGY LETTERS

from birth to division, similar to bacteria and fungi (Fig. 1d). To determine which model of the three models—timer, sizer or adder—best described the data for *H. salinarum*, we examined the relationship between cell lengths at birth and division. If the sizer model was true, $l_{\rm birth}$ and $l_{\rm division}$ would be uncorrelated, yielding a slope of 0 from simple linear regression⁴. By contrast, the adder model predicts that cell size at birth is linearly related to the size at division with a slope of 1, because a constant length (Δ) is added between cell birth and division⁴, as described by the following equation:

$$l_{\text{division}} = l_{\text{birth}} + \Delta \tag{3}$$

In the timer model, one could assume that a newborn cell grows for one doubling time (that is, the constant time due to the exponential growth of single cells) before division. In this regime, we would expect a slope of 2 when a simple linear regression is applied to the birth size and division size, while infinitely broadening the cell size distributions⁴ (see Supplementary Notes Section 1 for more details). Regression analysis of the cell length data (Fig. 2a) using equation (3) yielded a slope of 0.88 ± 0.06 (s.e.; P < 0.001), and regression of the 2D area data (Supplementary Fig. 4b) gave a slope of 0.98 ± 0.07 (s.e.; P < 0.001). These results suggest that the adder model best describes cell size control in H. salinarum.

Furthermore, we found that birth length and interdivision time are negatively correlated (Fig. 2b). In fact, the adder model predicts this negative relationship between birth size and interdivision time (Fig. 2b). The prediction from the adder paradigm and experimental data are well aligned for both cell length (Fig. 2b) and 2D area data (Supplementary Fig. 4c). As expected, we also found that the added size (Δ) between birth and division remains unchanged, regardless of the birth size (Fig. 2c and Supplementary Fig. 4c), further supporting

the adder model. From the analysis in Fig. 2 and additional experimental evidence (Supplementary Figs. 4 and 6), we concluded that cell size control in *H. salinarum* follows the adder model.

While the adder model best describes the H. salinarum data (Fig. 2 and Supplementary Fig. 4), single-cell imaging data also revealed important biological fluctuations in the archaeal cell cycle that affect size control (Fig. 3a). In particular, we found that the cell division placement is noisier in H. salinarum cells than in E. coli (that is, the standard deviations of division ratio distributions are 0.03 and 0.01, for H. salinarum and E. coli, respectively), indicating that division placement is more likely to deviate from the exact midpoint of archaeal cells (Fig. 3b,c). The distribution of exponential growth rate of individual H. salinarum cells was also broader than that of E. coli cells (Fig. 3d). The CV of the exponential growth rate distribution was 17% for H. salinarum, whereas the CV for E. coli distribution is reported to be as low as 8% in fast growth environments6. The latter quantity is reported to be as low as 10% in a microfluidics setup, showing that the statistics are comparable between different experimental setups (see Supplementary Notes Section 8 for further data and discussion). Together, these data demonstrate that relative magnitudes of the noise in cell division ratio and growth rate of H. salinarum are 2-3-fold larger than those of E. coli. Although these differences in the noise terms might initially seem negligible, we found that they influence cell size control in *H. salinarum*.

Specifically, we computed Pearson correlation coefficients between different cell cycle parameters (Supplementary Table 3) for *H. salinarum*. Previously, theoretical⁴ and experimental^{5,6} studies for *E. coli* cells showed that the correlation between $l_{\rm birth}$ and $l_{\rm division}$ is 0.5 for the adder model (Supplementary Table 4), assuming a perfectly symmetrical cell division and accounting for random noise in interdivision time. Thus, for *E. coli*, the variances of growth rate

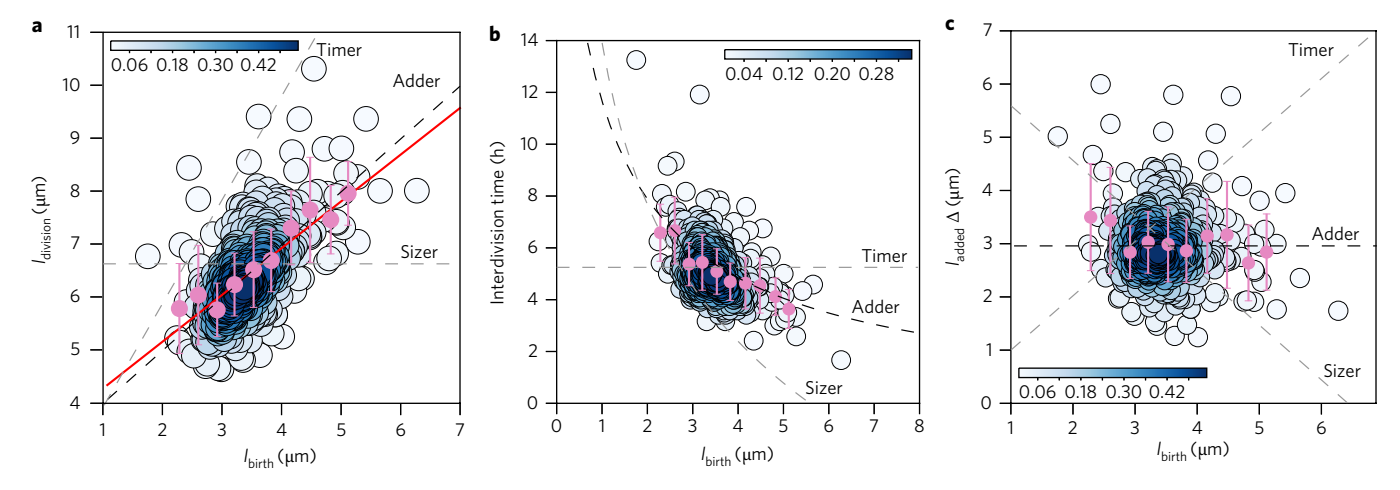
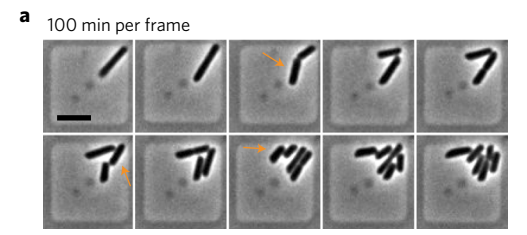
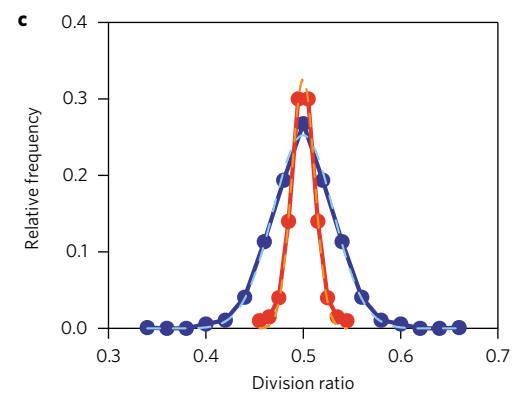


Fig. 2 | H.salinarum cells effectively add a constant length between generations, consistent with the adder model. a, Cell lengths at birth and division are linearly related, and linear regression of the raw data (red solid line) yields a slope of 0.88 ± 0.06 (s.e.; 95% CI:0.8-1, n = 418, P < 0.001 for the null hypothesis that the slope is zero). A black dashed line with a slope of 1 represents the theoretical line for the adder model. Grey dashed lines with a slope of 2 and 0 are shown to represent the theoretical lines for the timer and sizer models, respectively. **b**, Given the exponential growth at the single-cell level (Fig. 1c and Supplementary Fig. 4a), equation (2) can be expressed as: $t_d = \frac{1}{\lambda} \ln(1 + \frac{\Delta}{l_{\text{birth}}})$ (referred to hereafter as equation (7)) after substituting in equation (3). By inserting independently determined λ and Δ into equation (7), we arrive at a precise inverse relationship between l_{birth} and t_d . Birth length and interdivision time are negatively correlated, and the binned data closely match the theoretical prediction for the adder model (black dashed line) (equation (7)), which has no adjustable parameters. Theoretical lines for the timer and sizer models are shown as grey dashed lines. The line for the timer model has a slope of 0. For the sizer model, $t_d = \frac{1}{\lambda} \ln(\frac{c}{\lambda} \frac{l_{\text{birth}}}{l_{\text{birth}}})$ was plotted. **c**, A constant length is added regardless of the birth length. Pearson correlation coefficient of birth length and added length was -0.1 (n = 418, 95% CI: -0.2 to -0.0004). The small magnitude of the coefficient indicates that there were no significant relationships between these parameters. As expected, the binned data closely match the theoretical prediction for the adder model (black dashed line). Theoretical lines for the timer and sizer models are shown as grey dashed lines. The line for the timer model has a slope of 1, assuming that the cell doubles in size to keep a constant doubling time. For the sizer model, Δ

LETTERS NATURE MICROBIOLOGY







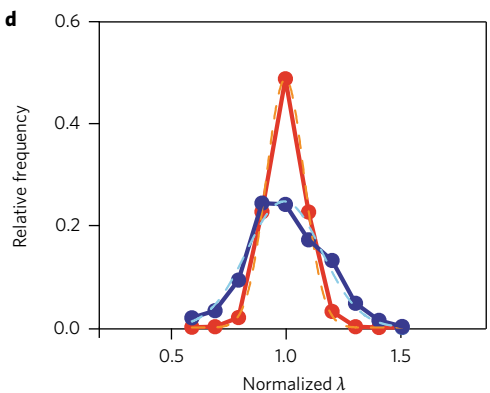


Fig. 3 | Distributions of division ratio and exponential growth rate of H. salinarum cells are broader than those of E. coli. a, Noisy symmetric division of mother cells often leads to two daughter cells of different lengths. An example montage of division events is shown. Longer daughter cells are indicated by orange arrows. Scale bar, 5 µm. **b**, Schematic explaining how noisy divisions were quantified using the division ratio. A perfectly symmetric division would give a ratio of 0.5. c, Histograms depict the division ratio distributions of H. salinarum cells (blue; pooled from three trials) and E. coli cells (red; data from ref. 9). Gaussian fit of each distribution gave standard deviations of 0.03 and 0.01, for H. salinarum (light blue dashed line) and E. coli (orange dashed line), respectively (n = 418 for H. salinarum, $R^2 = 0.99$ for both organisms). d, Histograms depict the distribution of exponential growth rates of individual H. salinarum cells (blue; CV of 17%; pooled from three trials) and E. coli cells (red; CV of 8%; analysed published data⁷). The CV for E. coli is similar to previous studies^{6,8}. Gaussian fit of each distribution gave standard deviations of 0.16 and 0.08, for H. salinarum (light blue dashed line) and E. coli (orange dashed line), respectively (n = 418 for H. salinarum, $R^2 = 0.96$ and 0.99 for H. salinarum and E. coli, respectively). The growth rates were uncorrelated between mother and daughter cells in H. salinarum, similar to previous studies in E. coli³³ (Pearson correlation coefficient: -0.1, 95% CI: -0.2 to 0.01, P=0.1).

and division ratio distributions are small enough that the simpler framework requiring interdivision time noise only was sufficient to capture experimentally observed correlations through simulations (Supplementary Table 4). By contrast, this and other correlations for *H. salinarum* were found to deviate from the model predictions (Supplementary Table 3), indicating that the previously proposed framework^{2,4} is insufficient to capture the larger biological noise observed in the *H. salinarum* cell cycle (Fig. 3) and that the higher magnitude of the noises affect the correlations between different cell cycle parameters.

Thus, we developed a theoretical framework (see Methods and Supplementary Notes Sections 2 and 3 for details) that includes two additional stochastic variables; namely, the variables included were noise in division ratio, interdivision time and exponential growth rate (Fig. 4a). Noise in division ratio (σ_{ratio}) describes the experimental observation that the division placement of *H. salinarum* cells is not always at the exact midpoint of the cell (Fig. 3). Similarly, each newborn cell would have its exponential growth rate randomly drawn from a distribution whose variance is described with the noise in exponential growth rate (σ_i) (for example, Fig. 3d). The third noise variable in the model is $\sigma_{\mbox{\tiny time}},$ which describes the spread of the distribution for time noise (t_{noise}). In theoretical frameworks published previously^{2,4}, this was the only noise term that was required to adequately explain experimental data for E. coli (Supplementary Table 4). The actual interdivision time measured for a given cell can be described as the sum of a target interdivision time necessary to precisely add a constant volume (Δ) plus some time noise, which causes the actual interdivision time to deviate slightly from the target interdivision time $(t_{\text{target}})^4$.

Simulated correlation coefficients based on our framework matched well to experimental coefficients measured for *H. salinarum* (Fig. 4b, Supplementary Table 3 and Supplementary Notes Section 5). The dramatically improved agreement relative to previous instantiations of the adder model^{2,4,24–26} (Fig. 4b and Supplementary Table 3) demonstrates a more general use of our extended framework for capturing relevant biological fluctuations across a wide diversity of species than previous models. In addition, this result indicates that noise in division ratio, interdivision time and exponential growth rate appreciably influence the adder model and cell size distributions. Interestingly, the correlation between the birth size of mother and the birth size of daughter cells was the only relationship unaffected by the presence of any of the noise terms (Supplementary Table 3 and Supplementary Notes Section 3).

To further examine the validity of our framework, we tested the prediction that the standard deviations of cell size distributions are equivalent to the standard deviation in interdivision time after appropriate scaling (see Supplementary Notes Section 2 for derivations). Indeed, these distributions from H. salinarum data collapsed after accounting for σ_{time} , σ_{ratio} and σ_{λ} (Fig. 4c and Supplementary Fig. 7). This prediction is in contrast to the experimental and theoretical evidence for E. coli cells, whose interdivision and cell size distributions could be scaled using σ_{time} alone^{2,4,6}. Thus, our coarse-grained framework showed that the adder model could accommodate several different biological fluctuations to maintain cell size homogeneity. This framework could be used as a diagnostic tool not only to recognize the implementation of the adder model in other organisms but also to help understand which noise terms prominently affect the correlations between different cell cycle parameters for the adder model. Interestingly, a recent study showed that mycobacteria actively control asymmetric division to create a more diverse population, making them less susceptible to antibiotics²⁷. Similarly, the various noise terms we studied here may have implications for the population growth.

In conclusion, our study demonstrates that an archaeal organism controls its cell size by adding a constant length between two

NATURE MICROBIOLOGY LETTERS

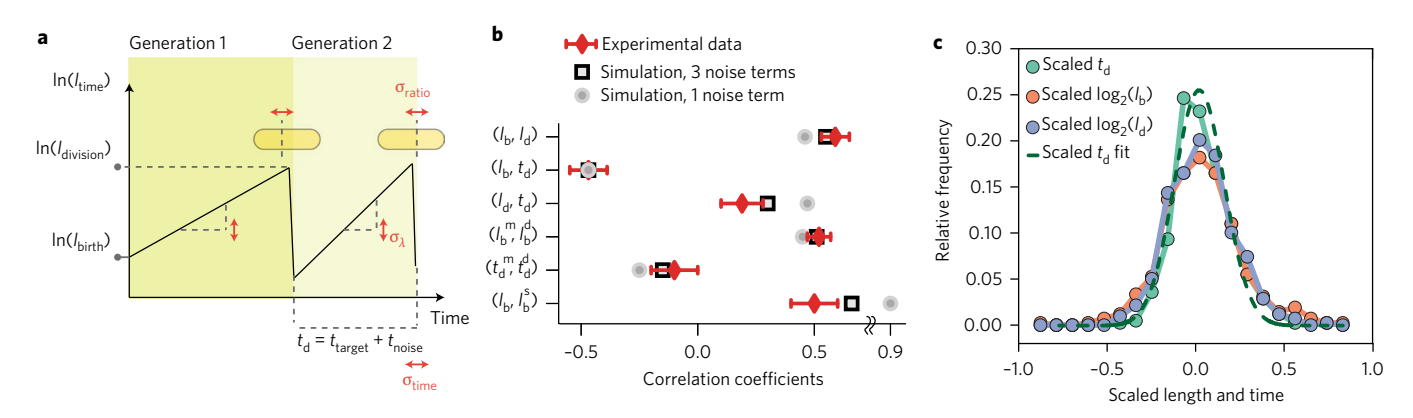


Fig. 4 | Noise in interdivision time, division placement and exponential growth rate significantly affect the archaeal cell size distribution. a, Schematic illustrating our theoretical framework. The cell growth cycle for two generations is depicted, with time on the x axis and the log of cell length at any given time on the y axis. The total interdivision time is the sum of an ideal interdivision time that is necessary to precisely add a constant length plus some time noise. Noise terms for division ratio, exponential growth rate and interdivision time are indicated by $\sigma_{\text{ratio'}}$ σ_{λ} and $\sigma_{\text{time'}}$ respectively. Red double-headed arrows indicate how each noise term leads to individual cells having different division ratio, exponential growth rate and interdivision time. For σ_{ratio} we have drawn a rod-shaped cell and its division placement to illustrate how this term governs how noisy the cell divisions are. Assuming the sample distribution shown in Fig. 3c accurately represents the true population distribution, every dividing cell would have its division ratio randomly drawn from a distribution like the one in Fig. 3c. Because of the fluctuations in division placement, the CV of birth length (16%) is bigger than the division length (13%) (Fig. 1d). For σ_{λ} , we show two cells with different growth rates (that is, the slope from I_{birth} to I_{division} is steeper for cell 2), which contribute to different interdivision times. b, We used correlation coefficients as a sensitive metric to evaluate our theoretical framework. Different pairs of interdivision time and cell length parameters used for correlation calculations are listed on the y axis. Subscripts b and d indicate birth and division, respectively. Superscripts m, d and s indicate generational relationships: mother, daughter and sister, respectively. Correlation coefficients from stochastic simulations (in black squares) incorporating σ_{time} , σ_{ratio} and σ_{λ} match well with the values derived from experimental data (n = 418 after pooling from three trials; error bars indicate 95% CI). Coefficients from a simulation that took only σ_{time} into account are shown in grey circles for comparison (based on the theory from ref. 4). The exact values for simulation and experimental correlation coefficients are tabulated in Supplementary Table 2. c, Length distributions can be collapsed with the t_d distribution after accounting for σ_{timer} σ_{ratio} and $\sigma_{\lambda r}$ as predicted by the theory (n = 418; see Methods and Supplementary Notes Section 2 for details). The t_d distribution was fitted using a Gaussian fit ($R^2 = 0.97$). For this plot, we pooled the data from three trials.

cell cycle events (Fig. 2 and Supplementary Fig. 4), but with higher variance in cell cycle parameters relative to bacteria (Fig. 3). This finding expands the list of organisms that implement the adder model for size control across all domains of life, despite the differences in terms of cell shape, cell wall, membrane, DNA replication, transcription, translation, cell division and cell cycle control¹⁵⁻²¹. It remains to be determined which molecular players and cell cycle events (for example, cell division or DNA replication initiation) implement the adder strategy in H. salinarum. Several studies in E. coli have suggested that cell cycle control occurs at the initiation of DNA replication rather than at cell division, which was recently shown to be consistent with the adder model^{28,29}. It is possible that initiation events are also important in H. salinarum. Given the unique evolutionary position of archaea blending characteristics of both bacteria and eukaryotes, our results serve as a useful foundation for understanding the molecular mechanisms and evolution of cell cycle control.

Methods

Strain used and general growth conditions. H. salinarum NRC-1 (ATCC700922) was used for all experiments. Cultures were prepared prior to microscopy at 42 °C with shaking at 200 rpm. Cells were grown at 37 °C in agarose chambers during live-cell microscopy. As a nutrient-rich medium, we used Complete Media (CM): 250 g NaCl, 20 g MgSO₄·7H₂O, 3 g trisodium citrate-2H₂O, 2 g KCl and 10 g Oxoid peptone.

Measuring distributions of cell sizes for Supplementary Table 1. Liquid cultures were grown in CM (2 ml) from single colonies until saturation. Cells were then diluted to an optical density at 600 nm (OD $_{600}$) of 0.05 in CM to grow the cells to the stages indicated in Supplementary Table 1. For imaging, 2 µl culture aliquots were immobilized on No. 1.5 cover glass under an agar pad (2% w/v). Phase-contrast images (200 ms exposure) were collected on a Nikon TI microscope equipped with a 6.45-µm-pixel Photometrics HQ2 camera and a Nikon ×100 numerical aperture (NA) 1.4 objective.

To segment phase-contrast images of cells, the MATLAB-based software Morphometrics to was used with the phase-contrast setting. The cell contours obtained were visually inspected, and any erroneous contours were removed. After segmentation of cells, two filters were created to eliminate any non-rod-shaped cells. A rod shape was defined as a cell that possesses two poles. Cells that were bent, instead of being straight rods, were detected by calculating the distance between two poles. For a straight rod cell, this distance should be the same as the cell length computed by Morphometrics. For the first filter, a threshold of 650 nm was placed on the absolute difference between the pole-to-pole distance and the cell length from Morphometrics, to identify bent rods that exceeded this threshold. A second filter was created to detect spherical or amorphous-shaped cells: the percentage of 'flat' regions (that is, very small local curvature) in the perimeter of each cell was calculated. This percentage was required to be >10% for a cell to be classified as a rod.

Fabrication of agarose microchambers. For microscopy analysis of H. salinarum single-cell growth, microchambers of $10 \times 10 \,\mu\text{m}^2$ squares with a $2 \times 2 \,\mu\text{m}^2$ post at the centre of the microchamber were designed and constructed (Fig. 1a). We used CleWin (Delta Mask) to design the chambers, and repeated the design to a total of 40,000 chambers per array replica. We previously described the process for fabricating microchannels and rod-to-sphere microchambers31. Briefly, silicon dioxide wafers were cleaned with isopropanol and acetone and repeatedly rinsed in double-distilled water (ddH2O). A 10:1 solution of hexadimethylsiloxane:i sopropanol was incubated on top of the clean wafer for 10 min. The solution was then spincoated, and the wafer was activated at 95 °C for 10 min to improve adhesion of photoresist. We then spincoated positive Shipley photoresist 1813 (MicroChem) and processed the photoresist film according to the manufacturer's instructions to obtain a layer thickness of 1.3 µm. The microchamber patterns were directly written onto the photoresists by applying laser lithography (µPG 101, Heidelberg Instruments). After exposure, the patterns were promptly developed by application of a small drop of MF-321 (MicroChem) for ~2 min on top of the array. The master was silanized overnight at room temperature by vapour deposition of heptadecafluoro-1,1,2,2-tetrahydrodecyl trichlorosilane (Gelest Inc.). Using soft lithography, the array pattern was replicated into polydimethylsiloxane (PDMS) (Sylgard 184) using a ratio of 10:1 (base:curing agent). The pattern was cured overnight in an oven at 65 °C while degassing, then peeled off from the silicon wafer. This PDMS mould was then used repeatedly to create agarose microchambers. We cleaned the mould from dust with adhesive tape and poured

LETTERS NATURE MICROBIOLOGY

a hot solution of agarose (4% w/v in water) to a thickness of \sim 5 mm. After the agarose was polymerized, a slab of agarose containing the microchamber arrays was cut (\sim 1.5 \times 1.5 cm²) and dialysed in 25 ml of CM with gentle agitation overnight to equilibrate the slab with growth media.

Time-lapse microscopy using agarose microchambers. Liquid cultures were grown from single colonies (2 ml CM at 42 °C with shaking at 200 rpm) until saturation, then diluted to an optical density of 0.05 in CM, and grown until exponential growth phase (OD₆₀₀ of \sim 0.7). At this point, we made a solution of low-melting agarose (4% w/v in water; Invitrogen, Cat. no. 15517-022) and kept this at 55 °C. We took 70 μl of cell culture, pre-incubated it at 55 °C for exactly 1 min and then mixed in 6 µl of the warm agarose solution (the final concentration of agarose was 0.32% w/v, and the final concentration of NaCl was 4.4 M). The agarose drop was placed on the tube sidewall to avoid cell lysis due to low osmolarity, and was mixed with cell suspension by vortexing. We then immediately spotted a 1 µl of the suspension on top of the patterned agarose slab and turned patterned-side down onto a cell culture dish with a glass bottom (MatTek, Cat. no. P50G-1.5-30-F) to trap cells inside the microchambers for time-lapse imaging. Cells inside the microchambers were imaged at 37 °C in a heated incubator that enclosed the microscope body. The total exposure time was 200 ms (100 ms exposure; 2 frames were collected and averaged), and the time interval was 5 min for the time-lapse (an average total duration of 20 h). Approximately 400 microchambers were imaged per trial, although not all chambers contained cells.

Image analysis of time-lapse movies to extract cell cycle parameters. To avoid imaging artefacts from phase-bright gas vesicles inside *H. salinarum* cells, individual cells were segmented manually using Fiji (ImageJ version 1.48r, NIH). Raw movies were cropped to one agarose chamber per image file. Cells were then segmented manually when they were born (that is, division of a mother cell) using the polygon tool in Fiji. Every segmentation was saved as a region of interest (ROI) using the ROI manager tool. These collections of ROIs for individual movies were then used as a template to generate artificial images that were fed into Morphometrics in MATLAB (R2012b).

Using Morphometrics, various cell shape parameters, including cell contour, length, width, area, pole locations and local curvature were calculated, and a unique ID was assigned for each cell to keep track of the ID of its mother and sibling cell. As described earlier, non-rod-shaped cells (that is, round and bent cells) were detected and excluded from the analysis, because the misshapen cells often underwent morphogenesis to become rods and were suspected to have different physiology from rod-shaped cells. When analysing growth, the length of rod-shaped cells can be used as a proxy for cell volume, as the change in the rod diameter during growth is small (CV of 12%; n = 92). The cell size of a mother cell at division was calculated by adding the cell sizes of its two daughter cells, and the division ratio was calculated by dividing the mother cell size by the cell size of a larger daughter cell. The cell size added was calculated by subtracting the birth size of the mother cell from its division cell size. The time taken from birth to division was calculated by subtracting the movie frame number at which birth happened from the frame number at which division occurred, and multiplying this by the acquisition rate of the movie (5 min between frames). The final data set of 418 mother cells was made by pooling the analysis from 3 independent trials.

Calculation of measurement precision and its effect on the division placement noise. To measure the precision of manual segmentation, we compared two sets of traces drawn for 74 individual cells. One set of traces was made in late 2015, and the other set in early 2017. The discrepancy between the two sets (that is, the measurement precision) was calculated to be $0.004\,\mu\text{m}^2$ for 2D cell area, and $0.01\,\mu\text{m}$ for cell length. We also confirmed that the two sets of traces were statistically identical by performing the Wilcoxon matched-pair test (two-tailed; P>0.6 for both 2D area and length), suggesting that the measurement noise is negligible.

In terms of the measurement precision for the automated segmentation in Morphometrics, we refer to two articles 32,33 that had developed the algorithm (that is, the subpixel cell detection algorithm) used in Morphometrics. The reported precision of the subpixel method is 0.0016 pixels² (6.6 nm²), which is three orders of magnitude smaller than the manual segmentation noise. Thus, the overall measurement noise is approximately $0.004\,\mu\text{m}^2$ for 2D cell area and $0.01\,\mu\text{m}$ for cell length.

Development of an analytical framework for the adder model with noisy symmetric divisions and noisy growth rates. The framework postulated that cells attempt to add a constant length from birth to division (equation (3)). The framework considered three sources of stochasticity: a time-additive noise in the time to division with standard deviation, $\sigma_{time}\tau$, noisy symmetric divisions with standard deviation σ_{ratio} and noisy growth rates with standard deviation, $\sigma_{\lambda} log_2/\tau$. Here, τ is the average doubling time.

We analytically obtained approximate distributions given by the model to the lowest order in the noise variables (see Supplementary Information for details). In particular, the CVs of cell size at birth, cell size at division and interdivision time were given by:

$$\sigma_x^2 = \frac{4}{3}(\sigma_{\text{time}}^2 + \sigma_{\text{ratio}}'^2) \tag{4}$$

$$\sigma_y^2 = \frac{4}{3}\sigma_{\text{time}}^2 + \frac{1}{3}\sigma_{\text{ratio}}^{\prime 2} \tag{5}$$

$$\sigma_{t_d}^2 = \frac{4}{3}\sigma_{time}^2 + \frac{1}{3}\sigma_{ratio}'^2 + \sigma_{\lambda}^2$$
 (6)

where $\sigma'_{\rm ratio} = \sigma_{\rm ratio} 2/ln_2$, $x = \log_2 \left(\frac{l_{\rm birth}}{\Delta}\right)$ and $y = \log_2 \left(\frac{l_{\rm division}}{2\Delta}\right)$; and σ_x and σ_y are the standard deviations of x and y, respectively. Pearson correlation coefficients between different cell cycle variables were also analytically approximated (see Supplementary Notes Section 3 for details). We extracted $\sigma_{\rm ratio}$, σ_x , σ_y and σ_{l_d} from experimental data. We used the CV of cell length at division, together with $\sigma_{\rm ratio}$ to extract $\sigma_{\rm time}$ using equation (5). Extracting $\sigma_{\rm time}$ from CV of cell length at birth using equation (4) and $\sigma_{\rm ratio}$ produced a consistent value for this noise term. We extracted σ_x using equation (6) with the measured CV of generation times (see Supplementary Notes Section 2 for details).

Simulation of *H. salinarum*. cell size distributions. We used numerical simulations (Python 2.7) of the stochastic model above to find *H. salinarum* cell length distributions and their CV. Simulations tracked l_{birth} , l_{division} and t_{d} of a growing and dividing cell for 10,000 generations. The starting cell had an initial cell length of 1, but the initial condition did not matter because the simulation reaches and maintains cell size homeostasis supplementary Fig. 6c). A simulated cell divided after growing for a time, $t_{\text{d}} = ln \left(1 + \frac{\Delta}{l_{\text{birth}}}\right) / \lambda + \sigma_{\text{time}} \xi$, where ξ is a normally distributed noise term with zero mean and unit variance. At division, the cell divided into two with a division ratio, $\frac{1}{2} + \sigma_{\text{ratio}} \xi$. Only one cell was kept for the next generation, which grew with a rate, $\frac{l_{\text{int}}}{\xi} + \sigma_{\lambda} \xi$. We set $\Delta = \tau = 1$ because we were interested in only dimensionless quantities, such as CVs and correlation coefficients. Note that all noise terms are independent (see Supplementary Notes Section 4).

Analysis of published data on E.coli. cell cycle. Single-cell growth data for the E.coli strain MG1655 from a published study⁷ were analysed according to published protocols, except that all data points whose cell size at birth was more than two standard deviations away from the mean were removed. The growth rate of a cell was then calculated as $ln\left(\frac{\text{division}}{l_{\text{birth}}}\right)/t_{\text{d}}$. Correlation coefficients between cell cycle variables for E.coli were calculated using data from four independent published experiments⁷. We used only the first 50 generations of cell growth to avoid ageing effects, and discarded the first 10 of the 50 generations to ensure steady state. The raw data contained a few outliers that strongly influenced Pearson correlation coefficients. We removed these outliers as shown in Supplementary Fig. 9. For each pair of variables, the correlation coefficients for each of the four experiments were computed independently, and averages and standard deviations of the four calculations are shown in Supplementary Table 4.

Life Sciences Reporting Summary. Further information on experimental design is available in the Life Sciences Reporting Summary.

Code availability. Python and MATLAB scripts used in this study have been deposited in the following url: https://bitbucket.org/garnerlab/.

Data availability. The data sets generated during this study are available from the corresponding authors (A.A. and E.C.G.) upon request.

Received: 8 February 2017; Accepted: 21 November 2017; Published online: 18 December 2017

References

- Deforet, M., van Ditmarsch, D. & Xavier, J. B. Cell-size homeostasis and the incremental rule in a bacterial pathogen. *Biophys. J.* 109, 521–528 (2015).
- Soifer, I., Robert, L. & Amir, A. Single-cell analysis of growth in budding yeast and bacteria reveals a common size regulation strategy. *Curr. Biol.* 26, 356–361 (2016).
- Sauls, J. T., Li, D. & Jun, S. Adder and a coarse-grained approach to cell size homeostasis in bacteria. Curr. Opin. Cell Biol. 38, 38–44 (2016).
- 4. Amir, A. Cell size regulation in bacteria. Phys. Rev. Lett. 112, 208102 (2014).
- Campos, M. et al. A constant size extension drives bacterial cell size homeostasis. Cell 159, 1433–1446 (2014).
- Taheri-Araghi, S. et al. Cell-size control and homeostasis in bacteria. Curr. Biol. 25, 385–391 (2015).
- Wang, P. et al. Robust growth of Escherichia coli. Curr. Biol. 20, 1099–1103 (2010).

NATURE MICROBIOLOGY LETTERS

- 8. Godin, M. et al. Using buoyant mass to measure the growth of single cells. *Nat. Methods* 7, 387–390 (2010).
- Guberman, J. M., Fay, A., Dworkin, J., Wingreen, N. S. & Gitai, Z. PSICIC: noise and asymmetry in bacterial division revealed by computational image analysis at sub-pixel resolution. *PLoS Comput. Biol.* 4, e1000233 (2008).
- Young, K. D. The selective value of bacterial shape. Microbiol. Mol. Biol. Rev. 70, 660–703 (2006).
- 11. Fievet, A. et al. Single-cell analysis of growth and cell division of the anaerobe *Desulfovibrio vulgaris* Hildenborough. *Front. Microbiol.* **6**, 1378 (2015).
- Iyer-Biswas, S. et al. Scaling laws governing stochastic growth and division of single bacterial cells. Proc. Natl Acad. Sci. USA 111, 15912–15917 (2014).
- 13. Banerjee, S. et al. Biphasic growth dynamics control cell division in *Caulobacter crescentus*. *Nat. Microbiol.* **2**, 17116 (2017).
- 14 Nobs, J. B., Maerkl, S. J. & Polymenis, M. Long-term single cell analysis of S. pombe on a microfluidic microchemostat array. PLoS ONE 9, e93466 (2014).
- Hawkins, M., Malla, S., Blythe, M. J., Nieduszynski, C. A. & Allers, T. Accelerated growth in the absence of DNA replication origins. *Nature* 503, 544–547 (2013).
- Herrmann, U. & Soppa, J. Cell cycle-dependent expression of an essential SMC-like protein and dynamic chromosome localization in the archaeon Halobacterium salinarum. Mol. Microbiol. 46, 395–409 (2002).
- Kelman, L. M. & Kelman, Z. Archaeal DNA replication. *Annu. Rev. Genet.* 48, 71–97 (2014).
- Duggin, I. G. et al. CetZ tubulin-like proteins control archaeal cell shape. Nature 519, 362–365 (2015).
- Lindås, A.-C. & Bernander, R. The cell cycle of archaea. *Nat. Rev. Microbiol.* 11, 627–638 (2013).
- Popławski, A. & Bernander, R. Nucleoid structure and distribution in thermophilic archaea. J. Bacteriol. 179, 7625–7630 (1997).
- Lundgren, M. & Bernander, R. Genome-wide transcription map of an archaeal cell cycle. Proc. Natl Acad. Sci. USA 104, 2939–2944 (2007).
- Zaremba-Niedzwiedzka, K. et al. Asgard archaea illuminate the origin of eukaryotic cellular complexity. Nature 541, 353–358 (2017).
- 23. Amir, A. Is cell size a spandrel? *eLife* **6**, e22186 (2017).
- 24. Ghusinga, K. R., Vargas-Garcia, C. A. & Singh, A. A mechanistic stochastic framework for regulating bacterial cell division. *Sci. Rep.* **6**, 30229 (2016).
- Osella, M., Nugent, E. & Cosentino Lagomarsino, M. Concerted control of Escherichia coli cell division. Proc. Natl Acad. Sci. USA 111, 3431–3435 (2014).
- 26. Kennard, A. S. et al. Individuality and universality in the growth-division laws of single *E. coli* cells. *Phys. Rev. E* **93**, 012408 (2016).
- Rego, E. H., Audette, R. E. & Rubin, E. J. Deletion of a mycobacterial divisome factor collapses single-cell phenotypic heterogeneity. *Nature* 546, 153–157 (2017).
- 28. Zheng, H. et al. Interrogating the *Escherichia coli* cell cycle by cell dimension perturbations. *Proc. Natl Acad. Sci. USA* 113, 15000–15005 (2016).
- Ho, P.-Y. & Amir, A. Simultaneous regulation of cell size and chromosome replication in bacteria. Front. Microbiol. 6, 662 (2015).

- Ursell, T. S. et al. Rod-like bacterial shape is maintained by feedback between cell curvature and cytoskeletal localization. *Proc. Natl Acad. Sci. USA* 111, E1025–E1034 (2014).
- Renner, L. D., Eswaramoorthy, P., Ramamurthi, K. S. & Weibel, D. B. Studying biomolecule localization by engineering bacterial cell wall curvature. *PLoS ONE* 8, e84143 (2013).
- Paintdakhi, A. et al. Oufti: an integrated software package for high-accuracy, high-throughput quantitative microscopy analysis. *Mol. Microbiol.* 99, 767–777 (2016).
- Sliusarenko, O., Heinritz, J., Emonet, T. & Jacobs-Wagner, C. Highthroughput, subpixel precision analysis of bacterial morphogenesis and intracellular spatio-temporal dynamics. *Mol. Microbiol.* 80, 612–627 (2011).
- 34. Wallden, M., Fange, D., Lundius, E. G., Baltekin, Ö. & Elf, J. The synchronization of replication and division cycles in individual *E. coli* cells. *Cell* **166**, 729–739 (2016).

Acknowledgements

We thank T. Ursell for Morphometrics, D. B. Weibel for providing a fabrication facility, and K. A. Dulmage, M. Kapoor and W. Marshall for stimulating discussions. This work was supported by a Searle Scholars Award and NIH grant DP2AI117923-01 to E.C.G.; a HHMI Helen Hay Whitney Foundation Fellowship to Y.J.E.; the Harvard MRSEC program of the NSF DMR 14-20570 to P.H.; an A. P. Sloan Foundation grant and a Kavli Foundation grant to A.A.; and an NSF grant MCB-141-7750 and Duke Arts and Sciences Research Council Committee on Faculty Research grant to A.K.S., A.A., L.D.R. and E.C.G. also acknowledge support from the Volkswagen Foundation.

Author contributions

Y.-J.E., A.S., E.G. and A.A. conceived and designed the experiments. Y.-J.E., M.K., L.D.R. and S.L. performed the experiments. Y.-J.E., P.-Y.H., L.R. and A.A. analysed the data. Y.-J.E., P.-Y.H. and A.A. developed and evaluated the theoretical framework. Y.-J.E., P.-Y.H., L.D.R., L.R., A.S., E.G. and A.A. wrote the manuscript.

Competing interests

The authors declare no competing financial interests.

Additional information

 $\label{eq:supplementary} \textbf{Supplementary information} \ is \ available \ for \ this \ paper \ at \ https://doi.org/10.1038/s41564-017-0082-6.$

Reprints and permissions information is available at www.nature.com/reprints.

Correspondence and requests for materials should be addressed to A.S. or E.G. or A.A.

Publisher's note: Springer Nature remains neutral with regard to jurisdictional claims in published maps and institutional affiliations.